ISSN 0030-400X, Optics and Spectroscopy, 2010, Vol. 108, No. 4, pp. 581–590. © Pleiades Publishing, Ltd., 2010.
Original Russian Text © S.I. Lysenko, B.A. Snopok, V.A. Sterligov, 2010, published in Optika i Spektroskopiya, 2010, Vol. 108, No. 4, pp. 618–628.

CONDENSED-MATTER SPECTROSCOPY

Scattering of Surface Plasmon–Polaritons and Volume Waves by Thin Gold Films

S. I. Lysenko[a, b], B. A. Snopok[a], and V. A. Sterligov[a]

[a] *Institute of Semiconductor Physics, National Academy of Sciences of Ukraine, Kiev, 03028 Ukraine*
[b] *Physics Department, University of Puerto Rico, Mayaguez, 00681 Puerto Rico, USA*
e-mail: snopok@isp.kiev.ua; b_snopok@yahoo.com

Received June 2, 2009

Abstract—The specific features of elastic scattering of volume waves and surface plasmon polaritons by polycrystalline gold films have been investigated. An analysis of the relative scattered energy, power spectral density of surface roughness, and integral and angular dependences of scattering of waves of different nature indicates a strong nonradiative multiple scattering of surface plasmon polaritons in gold films. When roughness increases, this scattering leads to an increase in scattering isotropy and to a partial loss of structural information about gold films. The analysis of the scattered energy of surface plasmon polaritons with application of the data on multifractal dimension of gold surface indicates also that the radiative scattering of surface plasmon polaritons depends on both the rms surface roughness and the surface wave propagation length.

DOI: 10.1134/S0030400X10040120

INTRODUCTION

Optical methods for studying the statistical properties of surface have become very popular in the recent years due to express analysis, nondestructive effect of probe radiation, and possibility to analyze structures of different physicochemical nature and spatial structure. Among many optical techniques a light scattering is one of the most informative for studying the statistical properties of spatial relief in a wide range of sizes of characteristic surface elements: from several nanometers to several hundreds of micrometers [1, 2]. Although this approach has been known for more than a century, its potential is far from exhausted. On the one hand, the appearance of many new objects with exotic properties, such as ensembles of quantum dots, metallic and semiconductor nanoparticles, and photonic crystals, puts new problems for applying light scattering and data obtaining on the properties of these objects by analyzing their interaction with light. At the same time, the new physical properties which are responsible for light localization in the surface region (for example, surface plasmon-polariton states), give additional possibilities for deriving this information.

In contrast to bulk electromagnetic waves, surface waves [3, 4] are localized in a thin surface layer, and their field strength decreases exponentially with increasing distance from the surface. Due to the difference in the electric and magnetic field vectors for surface and volume waves, these waves interact differently with matter. An analysis of these features provides unique information about the spatial structure at the interface, which cannot be derived by microscopy or other methods.

The electromagnetic field amplitude of a surface wave increases significantly if the latter is excited at the metal film/insulator interface at equal projections of the wave vector of the incident radiation and the wave vector of surface plasmon polaritons (SPPs) in the metal film. Although many studies have been devoted not only to the interaction between SPPs and surface relief but also to analytical applications of this approach, the numerous features of their SPP scattering by these structures still need to be investigated. In particular, along with single scattering, the excitation of SPPs on a metal surface may lead to multiple nonradiative scattering [5, 6].

The use of experimental methods for studying the SPP near field [7] allowed us to establish new features of SPP scattering, which lead to significant fluctuations of local electromagnetic field and are observed at certain sizes and shape features of relief inhomogeneities. Therefore, it is necessary to study the SPP scattering mechanisms as functions of the surface relief statistical characteristics to solve many scientific problems, which are related, in particular to the correct theoretical description of the interaction between electromagnetic waves and matter.

In this paper, we report a study of SPP scattering by the surfaces of polycrystalline gold films with different statistical properties of which are related to different modes of temperature treatment (low-temperature annealing). We considered the possibility of applying the classical theory of SPP scattering for samples with a low-scale roughness by comparing the data on the statistical properties of surface, derived from the information on scattering of SPPs and bulk electromag-

netic waves, and analyzing the atomic force microscopy (AFM) surface images.

This paper begins with a brief consideration of the theoretical bases of SPP scattering stochastic on reliefs, which is followed by the description of the experimental conditions. The analysis of the experimental results begins with the consideration of the correspondence between the data of the integrated intensity of scattered volume waves and SPPs and the rms roughness (AFM data) of the samples annealed at different temperatures. A more detailed analysis of the light scattering features using intensity indicatrices of scattered light in hemisphere is given in the next section. Finally, the results of the study are generalized with respect to the dominant mechanisms of scattering of bulk and surface waves.

SPP SCATTERING ON METAL SURFACES

An excitation of SPPs caused by resonant oscillations of the electron gas of conductor under the electromagnetic field of incident wave near the metal surface leads to the formation of charge density perturbation, i.e., a SPP [3]. SPPs are most often generated by light using the method of attenuated total internal reflection (ATIR) in the Kretschmann geometry [8] because this experimental technique is simple and highly reproducible. SPPs are resonantly excited under exposure of a metal film deposited on one of the faces of a transparent prism by *p*-polarized light at an angle of incidence θ_0, when the projection of the wave vector of light incident on the surface,

$$k_{||} = (\omega/c)\sqrt{\varepsilon_p}\sin\theta_0$$

(ε_p is the prism permittivity), is equal to the SPP wave vector. In accordance with the classical approach, in the absence of spatial modulation of ε_p, the surface relief plays a key role in the propagation of SPPs and partial transfer of their energy to the environment in the form of scattered light. The nature of this scattering has been discussed in many theoretical and experimental studies. The conventional approach to the description of SPP elastic single scattering on a metal surface with a small rms roughness δ_{rms} was reported in the theoretical studies by Kroger and Kretschmann (KK model) [9, 10].

The analytical expressions derived in these studies make it possible to calculate the statistical surface roughness parameters from the data on the spatial distribution of scattering intensity in the far zone. Within this model, the metal surface is considered as absolutely smooth, with a nonuniform distribution of the high-frequency surface polarization currents induced by incident light. The polarization currents are radiation sources, and the angular intensity distribution depends on the statistical features of the surface and optical constants of the medium. According to the KK model, the angular distribution of normalized intensity of light scattered from SPPs into a solid angle $d\Omega$ (angle-resolved scattering, ARS) can be written as

$$\begin{aligned}\mathrm{ARS}(\theta, \varphi) &= \frac{1}{P_{\mathrm{inc}}}\left(\frac{dP_{\mathrm{scat}}}{d\Omega}\right) \\ &= \frac{1}{4}\left(\frac{\omega}{c}\right)^4 \frac{\sqrt{\varepsilon}}{\cos\theta_0}\left|t^p(\theta_0)\right|^2 \left|W(\theta, \varphi)\right|^2 \mathrm{PSD}(\theta, \varphi),\end{aligned} \quad (1)$$

where θ_0 is the angle of incidence of probe radiation, θ and φ are the polar and azimuthal scattering angles, P_{inc} is the intensity of incident radiation, P_{scat} is the intensity of scattered radiation, ε is the permittivity of the metal film, $t^p(\theta_0)$ is the electric field amplitude gain on the surface, $W(\theta, \varphi)$ is the dipole radiation function, $\mathrm{PSD}(\theta, \varphi)$ is the power spectral density function of the surface roughness, and ω and c are the circular frequency and speed of light, respectively.

This dependence indicates that the spatial distribution of scattered light is determined by the product of the functions $W(\theta, \varphi)$ and $\mathrm{PSD}(\theta, \varphi)$. Many experiments on SPP scattering from the surface of a silver film were in satisfactory agreement with the KK theory. However, some experimental results [3, 4] could not be adequately described by dependence (1). The difficulty in interpreting the scattering data within the existing theory could be related to the multiple scattering processes, which were experimentally found later and investigated by scanning near-field optical microscopy (SNOM) [5, 7, 11].

One of the most interesting SNOM results is that multiple SPP scattering from a stochastic relief may lead to SPP localization in the surface plane. The effect of electromagnetic wave localization is similar to the Anderson electron localization in a strongly scattering medium. From the physical point of view the localization of electromagnetic waves is caused by multiple scattering and interference of waves, which may decrease the wave propagation velocity in the medium [12]. These surface features may reflect the dominant processes during film formation. The final surface relief has an internal structure, which is determined by the macroscopic conditions of film growth. The propagation of SPPs as surface electromagnetic excitations can reveal this hidden deterministic structure, leading to the formation of local peaks of electromagnetic field intensity in some crystal regions (hot spots). The size of these regions is much smaller than the SPP wavelength, because they are centers of spatial SPP interference on the stochastic relief. As was noted in [5, 7], the formation of localized states is accompanied by the SPP decay and emission of electromagnetic waves into the environment. Therefore, the processes of SPP localization may contribute to the general SPP scattering. However, there are no data on the intensity and spatial distribution of this scattering in the far zone.

EXPERIMENTAL

Samples

To carry out experiments on light scattering from a rough surface, we used gold films formed by vacuum deposition on the surface of quartz plates with a small rms roughness ($\delta_{rms} \sim 1.5$ nm). The gold films were prepared during one deposition cycle at a constant temperature (≈20°C), and therefore they had the same initial structure. Various statistical characteristics of the geometric surface relief were obtained by annealing at temperatures of 80, 120, 150, 200, and 250°C for 30 min. We studied these gold films by plasmon resonance spectroscopy with angular scanning and AFM and analyzed the features of light scattering from these films under the conditions of normal incidence (volume waves) and excitation of surface plasmon resonance [13].

Profilometry Studies of the Surface

The surface topography was investigated with a commercial AFM microscope (Nanoscope IIIa, Digital Instruments, Santa-Barbara, CA). The surfaces were scanned in the tapping force mode [14] using a commercial silicon nitride probe. A square surface area 1×1 μm in size was analyzed in one measurement cycle. The data were processed using the Digital Instruments software.

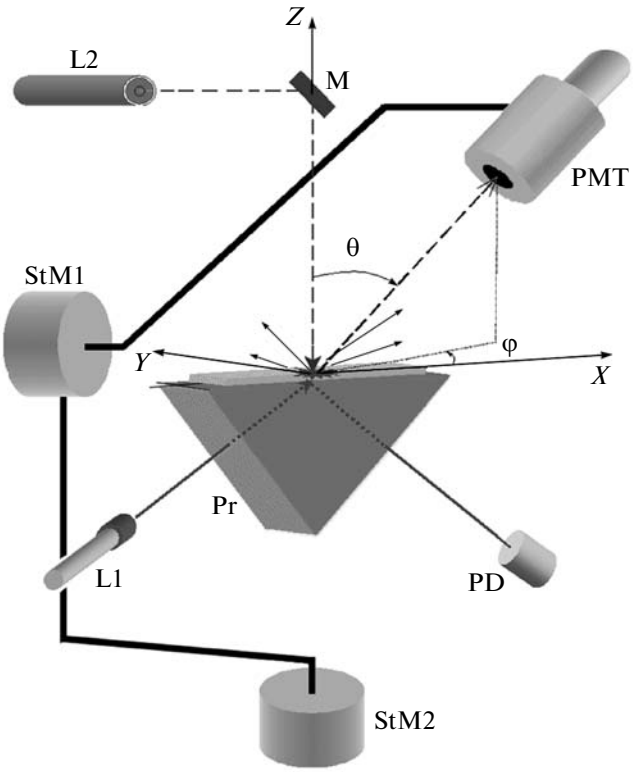

Fig. 1. Schematic of experimental setup for measuring scattering indicatrices.

Optical Measurements and Processing of Experimental Data

To numerically analyze the SPP scattering intensity distribution, the optical constants of gold films must be known. Hence, we measured the angular dependence of the light reflection coefficient under ATIR conditions. SPPs were excited on the film surface using *p*-polarized radiation of a He–Ne laser ($\lambda =$ 632.8 nm). A numerical approximation of the experimental angular dependence of the reflection coefficient by the theoretical dependence [4] allowed us to determine the real (ε') and imaginary (ε") components of the permittivity ε of the gold films and their thickness d_{ATIR}. We performed this approximation using original software. The accuracy of calculating the optical constants was determined by the degree of coincidence of the experimental and calculated angular dependences of the reflection coefficient. A comparison of the experimental and theoretical results gave an error in calculating ε', ε", and d_{ATIR} of less than 5%.

The experiment for studying the angular dependence of SPP scattering was performed on a setup shown in Fig. 1. Surface waves were excited in gold films in the Kretschman configuration using *p*-polarized radiation of L1 semiconductor laser (Modulated Laser Diode Module type 194-004 Radiospares Components, $\lambda = 670$ nm, 3 mW). A quartz plate with a deposited gold film was installed on the hypotenuse face of prism Pr using an immersion liquid (glycerol). The light intensity reflected from the gold film surface was measured by a PD photodiode (FD-24), which made it possible to find with high accuracy the angular position of the laser corresponding to the most effective SPP excitation.

In the experiment with bulk wave scattering, the sample was exposed to He–Ne L2 laser radiation ($\lambda =$ 632.8 nm). After reflection from the mirror M, the laser beam was incident normally to the surface and scattered from the relief irregularities.

The scattered light intensity was measured in both experiments by a photodetector, which included an analyzer, an objective with necessary diaphragms, and a photo multiply tube (PMT). An automatic angular displacement of the photodetector was implemented according to a specified algorithm using step motors StM1 and StM2. Thus, we obtained the angular dependences ARS(θ, φ).

Relationship between Scattering Angle and Spatial Frequency of Surface Relief

The shape of a rough surface can be presented as a 2D Fourier series. The light scattering by an individual component of this series with a specified spatial frequency *f* occurs in a certain direction. The relation

between the scattering direction and spatial frequency of the surface has the form [1, 2] $f = \Delta k/2\pi$ ($\Delta k = k - k_0$, k and k_0 are the tangential components of the wave vectors of the scattered and incident radiations, respectively). In the case of scattering of volume waves which incident normally to the surface, the tangential component of the incident wave vector k_0 is zero. Therefore, Δk becomes minimal at the scattering angle $\theta = 4°$ (the minimal scattering angle available for the measurement by setup) and maximal at the angle $\theta = 90°$, which corresponds to the spatial frequencies $f_{\text{BULKmin}} = \sin 4°/\lambda$ and $f_{\text{BULKmax}} = 1/\lambda$. When SPPs are excited on the gold film surface, the probe radiation is obliquely incident on the sample. In this case, the projection k_0 is nonzero and lies in the plane of incidence $\varphi = 0°$, 180°. The minimum and maximum values of Δk are obtained at the scattering angles $\theta = 90°$ and $\varphi = 0°$ or 180°, which correspond to the spatial frequencies [15]

$$f_{\text{SPP min}} = (\sqrt{\varepsilon_p}\sin\theta_0 - 1)/\lambda,$$

$$f_{\text{SPP max}} = (\sqrt{\varepsilon_p}\sin\theta_0 + 1)/\lambda.$$

It follows from these relations that the range of spatial surface frequencies that are available for studying upon SPP scattering is $\Delta f_{\text{SPP}} = f_{\text{SPP max}} - f_{\text{SPP min}} = 2/\lambda$, which exceeds the corresponding value for bulk wave scattering by a factor of more than two: $\Delta f_{\text{BULK}} = f_{\text{BULK max}} - f_{\text{BULK min}} = 0.93/\lambda$.

RESULTS AND DISCUSSION

Relative Energy of Scattered Bulk and Surface Waves

One of the most widely used scalar and spatially independent characteristics of surface inhomogeneity is the rms surface roughness δ. In the case where $\delta \ll \lambda$, bulk wave scattering is characterized by the following simple relation between the total integrated scattering (TIS) and δ value found from the data of [1, 2, 16]:

$$\delta_{\text{TIS}} = (\lambda/4\pi)\sqrt{\text{TIS}}, \quad (2)$$

where

$$\text{TIS} = \frac{1}{R}\int\int \text{ARS}(\theta, \varphi)d\theta d\varphi, \quad (3)$$

and R is the specular reflection coefficient for volume waves. Having introduced the relative scattered energy (RSE) as

$$\text{RSE} = \int\int \text{ARS}(\theta, \varphi)d\theta d\varphi,$$

we can write

$$\text{TIS} = \text{RSE}/R. \quad (4)$$

It is of great interest to compare the processes of scattering of bulk and surface waves from the same surface area in order to derive additional information about the surface properties. However, in the case of surface wave scattering, the use of relation (3) meets some problems. Indeed, for the SPP excitation, the balance distribution of the incident beam energy includes also the Joule loss upon nonradiative SPP decay. This loss can be qualitatively estimated by taking into account that the specular reflection coefficient beyond the SPP resonance condition is about 70–90%, whereas upon SPP excitation, it may decrease to a few percent or even less. At the same time, the part of the total incident energy transformed into scattered light does not exceed few percent. Thus, the fraction of the energy transformed into Joule loss is several dozen percent, which greatly exceeds the loss upon light scattering and violates relation (2) for surface wave scattering. To perform an adequate integral analysis of the processes of surface and bulk wave scattering, it is necessary to compare the measured RSE values. This will be done below.

The values of RSE_{SPP} for surface waves (λ = 670 nm) and RSE_{BULK} for volume waves (λ = 632.8 nm) were calculated from the experimental data ARS(θ, φ). Since the wavelengths of the radiation used to excite bulk and surface waves were fairly close, their difference will be neglected in our subsequent comparison of RSE_{BULK} and RSE_{SPP}.

The experimentally obtained RSE_{BULK} and RSE_{SPP} values are presented in Fig. 2 as functions of the film annealing temperature. It can be seen that the relative scattered energy for volume waves is approximately an order of magnitude lower in comparison with that for surface wave scattering. The most likely reason for this difference is the local field amplification under SPP excitation. According to [17], this amplification can be found from the angular dependence of the integrated scattering intensity: the ratio of the scattering intensities far from the resonance and in the resonance yields the local field amplification. The data of [17] for a sample with a similar structure show that the local field increases in resonance by approximately an order of magnitude, which corresponds to the observed difference in the RSE_{BULK} and RSE_{SPP} levels.

The RSE_{BULK} data were used to calculate the δ_{TIS} values, and the latter were compared with the AFM data on the rms roughness δ_{AFM}. The results for the gold films annealed at different temperatures are also shown in Fig. 2. The δ_{TIS} and δ_{AFM} values were measured using different physical methods based on the interaction with the sample surface: scattering of the luminous flux and the AFM probing. In addition, we should note the following. The data for calculating δ were also obtained for different spatial frequency ranges: $\Delta f_{\text{BULK}} = 0.11–1.58\ \mu\text{m}^{-1}$ for the bulk wave scattering, while the AFM analysis was performed for

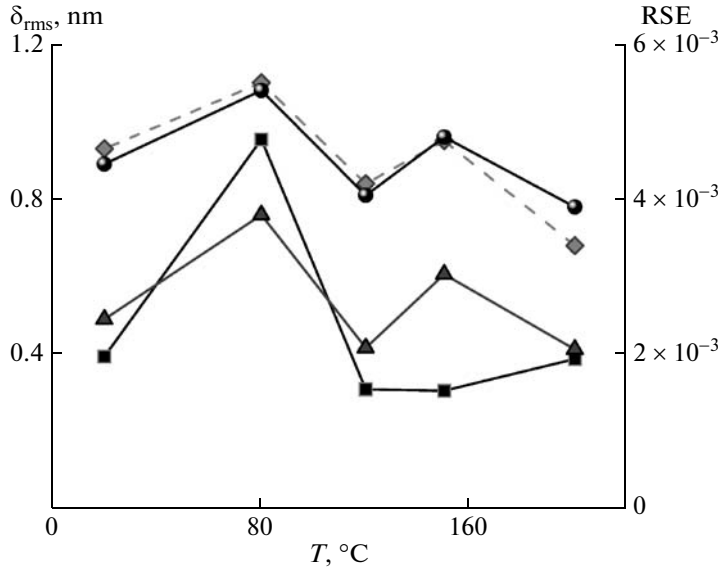

Fig. 2. Dependences of rms surface roughness δ_{rms}, found from bulk wave scattering (δ_{TIS}, circles) and AFM (δ_{AFM}, rhombs) measurements, and relative scattered energy for bulk (RSE_{BULK}, triangles) and surface (RSE_{SPP}, squares) waves on annealing temperature T of gold films. The RSE_{BULK} data are shifted by an order of magnitude.

the range $\Delta f_{AFM} = 1–256\ \mu m^{-1}$. However, the obtained δ values are fairly close, which apparently indicates that the spatial frequency range that is common for these two methods makes a dominant contribution to the measured δ value. Obviously, the proximity of the δ values obtained indicates the high reliability of the methods used.

The dependences in Fig. 2 allow one to select some characteristic features, which differ the light scattering by SPPs from the processes involving volume waves. A comparison of these dependences indicates that the SPP radiative decay depends more strongly on the annealing temperature than, for example, bulk wave scattering. Moreover, whereas the δ_{TIS} and δ_{AFM} data are in good correspondence in the entire temperature range under study, RSE_{SPP} exhibits qualitative differences at temperatures above 120°C. As was noted above, the dependences for δ_{TIS} and δ_{AFM} are in agreement, despite the difference in the spatial frequency ranges. Hence, we can suggest that, from the point of view of volume waves, gold films are spatial objects with averaged optical characteristics, which correspond to the effective values characterizing the interface. In other words, polycrystalline gold films can be considered as flat metal surfaces with effective optical parameters, which contain centers of elastic bulk wave scattering; the distribution of these centers is determined by the annealing temperature. In this case, the external surface relief is equivalent for both AFM and light scattering studies.

In the case of SPP generation, the processes of the interaction of electromagnetic radiation with matter are radically different: in fact, not only the surface, but also the entire film volume determines the formation of electron density distribution in the system. Since the field is amplified mainly near the outer metal surface, the relief features play a peculiar role in radiative SPP scattering. To analyze this question in more detail, it is necessary to use the data on the gold surface structure [13] because taking into account only such a scalar characteristic of the surface as the rms roughness seems to be insufficient in the consideration of SPP scattering processes. Indeed, in the case of volume waves both the surface and probe radiations are azimuthally isotropic: the absence of preferential direction both in the probe beam and in the distribution of reflecting faces at the interface determine the scattering intensity, which only depends on the relief depth. The presence of an isolated azimuthal direction upon SPP generation and its direct relationship with the electron density distribution in the film require more informative methods for describing the surface. As was noted above, the films under study are polycrystalline, with a developed surface and relief elements that range in size from several nanometers to several tenths of a micrometer. The dominant elements are gold crystallites 30–40 nm in diameter with a small-scale roughness [13]. Under these conditions, the use of multifractal analysis for surface characterization appears to be most justified because we are primarily interested in the statistical distribution of objects with different characteristic sizes on the surface, which can affect SPP propagation. A multifractal dimension makes it possible to estimate the dispersion of spatially invariant surface objects, which reflect the

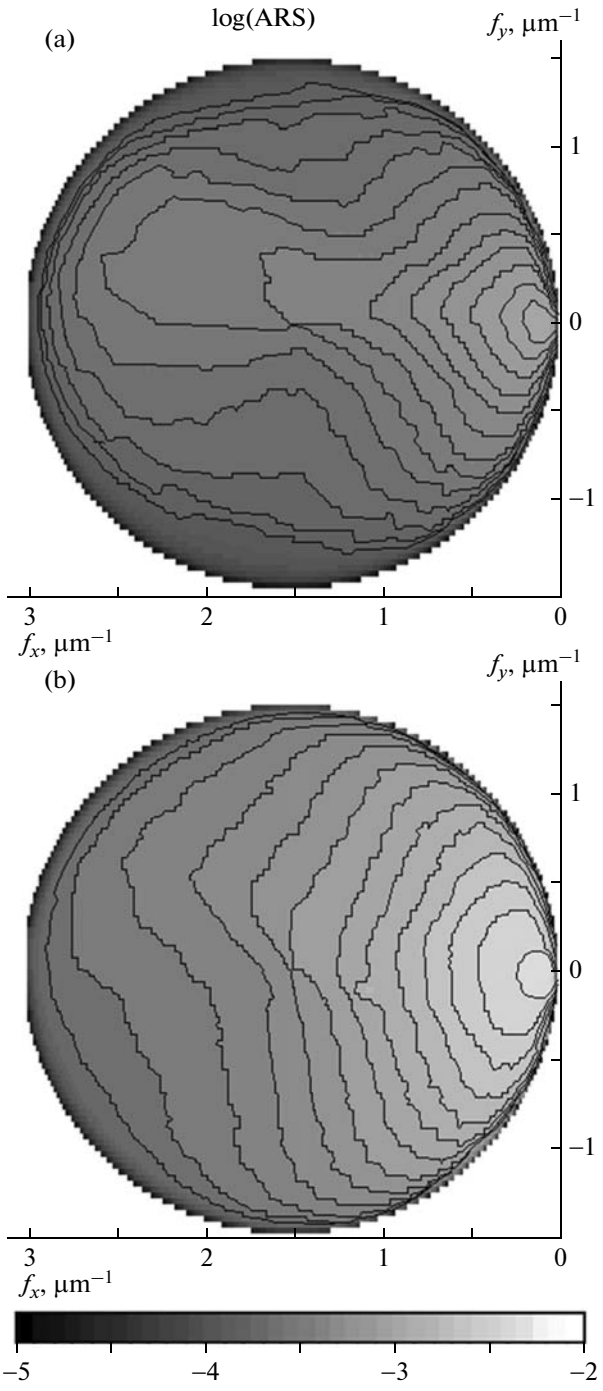

Fig. 3. SPP scattering indicatrices on gold film surface with changed surface topography (δ_{AFM} = (a) 9.5 and (b) 10.1 Å) as a result of low-temperature annealing at T = (a) 150 and (b) 80°C. The solid lines (isophots) correspond to a certain ARS value.

processes of film growth or subsequent treatment. In other words, a decrease in the multifractal dimension leads to a more homogeneous surface and lower light scattering from this surface due to the (i) longer SPP free path and (ii) lower probability of hot spot formation in the spatial distribution of electromagnetic field.

The RSE_{SPP} value is in good agreement with the results of calculation of multifractal dimension as a function of the annealing temperature [13]. The sharp decrease in the multifractal dimension in the range of 120–150°C corresponds to the decrease in the scattering intensity in the same temperature range. The reason is that a structural transformation occurs at temperatures of about 120°C, which leads to the disappearance of small-size roughness, i.e., to a smoother surface (several units of nanometers), without affecting the film structure on the larger scale, which make a decisive contribution to the rms roughness. In general, we can state the following: since a plasmon-polariton wave is involved in many events of elastic nonradiative scattering in the substrate plane during its motion, the radiative decay intensity depends on both the rms roughness δ and the surface wave propagation length. Both of these factors depend on the statistical relief features, which are sensitive to the conditions of film growth and subsequent treatment.

Spatial Distribution of SPP Scattering within a Hemisphere

The studies of the SPP scattering distribution into a hemisphere above the sample surface showed that an increase in the scattering intensity leads to a systematic change in its angular distribution. Therefore, we chose the indicatrices corresponding to the maximum and minimum integral SPP scattering for the analysis. As can be seen in Fig. 2, the SPP scattering intensity is maximum for the gold film annealed at 80°C and minimum for the film annealed at 150°C. The indicatrices of SPP scattering into a hemisphere for these films are shown in Fig. 3 as functions of the spatial frequencies f_x and f_y of the 2D expansion of the surface relief. They have a characteristic maximum in the plasmon propagation direction at low spatial frequencies f_x and f_y. This maximum is caused by (i) the monotonic increase in the dependence PSD(f_x,f_y) with a decrease in the spatial frequency and (ii) the contribution of the decrease in the projection of the illuminated area of the surface studied on the direction of observation [18].

Although the scattering intensity decreases monotonically with an increase in f_x, the indicatrix isophots in Figs. 3a and Fig. 3b differ significantly in shape. In Fig. 3a, when f_x increases to 1.5 μm, the isophots are narrowed to the plane of incidence, which is also accompanied by the formation of an additional weak maximum in the spatial frequency ranges f_x = 1.5–2.8 μm and f_y = –0.6–1 μm. At the same time, in the case of SPP scattering on the gold surface annealed at 80°C (Fig. 3b), this maximum is absent. Isophots do not demonstrate such an elongation as in Fig. 3a, and their shape approaches the arcs of concentric circles

with a center located near the origin of coordinates f_x and f_y.

As was noted above, the annealing of films at temperatures above 120°C leads to a significant decrease in the small-scale roughness with characteristic sizes of irregularities below the light wavelength. Thus, based on the data obtained, we can state that, at low annealing temperatures, when the system is mostly characterized by a small-scale roughness, scattering is stochastized in a peculiar way and, as a consequence, the structural information about the system is lost. This manifestation of light scattering from SPPs can be caused in particular by the increase in the intensity of multiple nonradiative SPP scattering in the surface plane.

Along with the SPP transformation into Joule heat, SPP radiative decay is the final event of the processes of multiple nonradiative scattering and propagation of SPPs in the surface plane. Nonradiative SPP scattering occurs most effectively, specifically from a small-scale roughness [3], and an increase in the number of these scattering events may lead to a significant deviation of the direction of SPP propagation from a straight line. As a result, this change in the character of SPP propagation should increase the isotropy of the measured scattering indicatrix; this is observed for the film annealed at 80°C, which has the most stochastic surface relief (Fig. 3b).

For smoother films annealed at temperatures above 120°C, the narrower isophots of the scattering indicatrix (Fig. 3a) indicate a smaller contribution of multiple nonradiative scattering to the SPP propagation.

Power Spectral Density Functions of Surface Roughness of Gold Films

Along with the scalar rms roughness, one of the main statistical surface characteristics is the power spectral density function of the PSD roughness. This function can be calculated from the experimental data within the existing theories [1, 2, 10] from both the bulk wave scattering and SPP scattering. When the permittivity of the gold film surface is homogeneous, the PSD functions calculated from the scattering data for different waves should characterize only the relief inhomogeneity and coincide. However, as was noted above, one might expect a manifestation of multiple scattering for SPPs, which may decrease the propagation velocity and give rise to local hot spots in the electromagnetic field distribution. As a result of this scattering, the PSD functions calculated from the SPP scattering data may differ from the similar functions derived from the bulk wave scattering data. Therefore, a comparison of these functions can yield additional useful information about the character of interactions of SPPs and bulk electromagnetic waves with the film inhomogeneities.

ATIR and AFM data on the permittivity ε and gold film thickness d

Annealing temperature, °C	ε (670 nm)	d_{ATIR}, nm	d_{AFM}, nm
20	$-14.56 + i0.99$	40.2 ± 2.0	39.6
80	$-14.45 + i1.20$	37.0 ± 1.8	38.4
120	$-14.10 + i1.18$	41.3 ± 2.1	42.8
150	$-13.91 + i0.89$	41.8 ± 2.1	43
200	$-13.55 + i1.01$	39.4 ± 2.0	38

To calculate the PSD functions from the SPP scattering data, we measured the polar diagrams of SPP scattering in the plane of incidence of probe radiation (Fig. 4). It can be seen that these diagrams differ significantly. The gold surface annealed at 80°C exhibits a sharp increase in the scattering intensity in comparison with the scattering by other surfaces. With a rise in the annealing temperature to 120 and 150°C, the scattering intensity decreases and then increases with a further rise in temperature to 200°C; the latter stage is accompanied by a change in the angular position of the indicatrix maximum. This change in the scattering characteristics indicates a significant change in the surface topography and possibly the thicknesses of the films studied (caused by the low-temperature annealing of the films).

To calculate the PSD functions, we found the permittivity ε and thickness of the gold films under study from the experimental angular dependence of the reflection coefficient R_{SPP} under ATIR conditions. An approximation of the experimental R_{SPP} data by the theoretical dependence allowed us to calculate the values of ε and film thickness d_{ATIR} (table). Since the experiments on SPP scattering were performed using a laser with $\lambda = 670$ nm, whereas the optical constants were obtained for $\lambda = 632.8$ nm, the necessary values ε(670 nm) were found by extrapolating the obtained ε(632.8 nm) values using the data in the literature [19] on the tendency of change in the spectral dependences of the optical constants of gold.

The gold film thicknesses d_{AFM} were also derived from the AFM measurements. To this end, a cavity was etched in each film by the lithographic method with a depth equal to the film thickness. The cavity depths were measured in different film regions using AFM; the results of subsequent averaging of the AFM data gave the d_{AFM} values (see table). It can be seen that the d_{ATIR} values are in agreement with the d_{AFM} data within the calculation error. Thus, the results obtained indicate a fairly high accuracy in determining the gold film parameters according to the ATIR data. Hence, one can use the obtained thicknesses and optical constants to calculate the PSD functions from the scattering indicatrices.

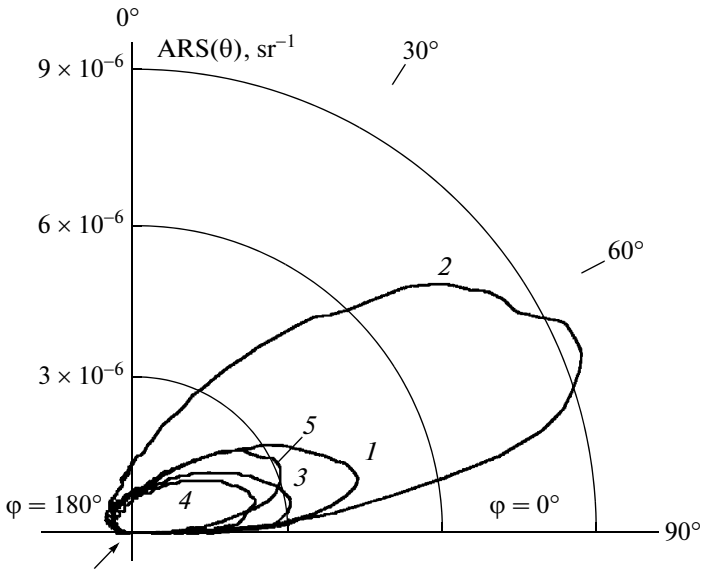

Fig. 4. Angular distribution of SPP scattered radiation. Arrow indicates incident radiation direction. Annealing temperature $T =$ (*1*) 20, (*2*) 80, (*3*) 120, (*4*) 150, and (*5*) 200°C.

The technique for calculating the PSD function of a surface on the basis of elastic bulk wave scattering and analysis of the angular dependence of scattering within the Elson theory [20, 21] is well studied and adequately describes the scattering process. Therefore, we used it as a control method for determining the PSD function. The experiments on the bulk wave scattering from the surface of annealed gold films showed an azimuthal isotropy of the scattering intensity, indicating an isotropic distribution of surface inhomogeneities. In this context, we analyzed only the polar dependences of the normalized scattering intensity ARS(θ), which were measured at a fixed azimuthal angle. Using these dependences, we calculated (within the vector scattering theory [22]) the power spectral density functions PSD_{BULK} of roughness for the gold films annealed at different temperatures (Fig. 5).

As was shown in [23], the interaction between SPPs and bulk inhomogeneities of metal film makes a small contribution to the SPP scattering; therefore, their effect on the intensity and angular distribution of scattered light was neglected. The dependences of SPP scattering ARS(θ) (Fig. 4) were used to calculate (within the KK model, with application of expression (2)) the power spectral density functions PSD_{SPP} for the roughness, which are shown in Fig. 5. The PSD_{SPP} and PSD_{BULK} values were calculated using the permittivity ε and thickness d_{ATIR} of the gold films. Additional calculations of PSD_{SPP} and PSD_{BULK}, in which ε was varied within several dozen percent demonstrated that the possible errors in ε could not change the behavior of PSD dependences.

Since the functions PSD_{BULK} and PSD_{SPP} describe the relief statistics for the same surfaces, they should coincide in the case of identical scattering mechanisms. However, their comparison shows that PSD_{BULK} and PSD_{SPP} depend differently on the relief spatial frequency f. The functions PSD_{SPP} rapidly decay with an increase in f, in contrast to PSD_{BULK}, which demonstrate no sharp falloff.

With allowance for the fact that the technique used to obtain the functions PSD_{BULK} was justified in [20, 21], the real surface function PSD should be most close to PSD_{BULK}. The discrepancy between the calculated roughness functions PSD_{BULK} and PSD_{SPP} may indicate some characteristic features in the interaction between SPPs and relief inhomogeneities that were disregarded in the KK theory (within which the functions PSD_{SPP} were obtained): multiple scattering, which changes the SPP propagation direction, and the possible formation of hot spots in the spatial field distribution [5, 7].

As was shown above, the change in the surface wave propagation direction due to multiple nonradiative scattering may increase the scattering indicatrix isotropy (Fig. 3b). In addition, the most efficient nonradiative scattering, leading to a significant change in the SPP propagation direction, should occur from small-scale inhomogeneities whose lateral sizes are comparable to the surface wave length. Therefore, one would expect an increase in this scattering at high spatial frequencies; this increase is likely to lead to the observed difference in the calculated PSD_{SPP} and PSD_{BULK} values. As a result, scattering is stochastized and the measured radiative SPP scattering from inhomogeneities

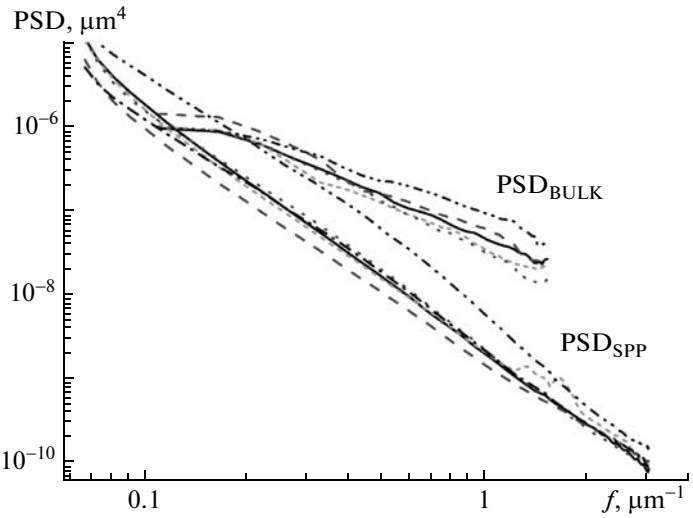

Fig. 5. PSD functions PSD_{BULK} and PSD_{SPP} for surfaces of gold films annealed at temperatures T = (—) 20, (–··–) 80, (- - -) 120, (– – –) 150, and (···) 200°C.

with high spatial frequencies in the measurement plane (plane of incidence) decreases.

An additional factor that may significantly affect the accuracy in determining PSD_{SPP} is the consideration of the SPP propagation length, which depends on the metal film structure. This dependence was demonstrated previously by direct near-field investigations on gold films [24]. Thus, the multiple nonradiative SPP scattering and the effect of the SPP propagation length can be the most likely reasons for the observed difference between PSD_{SPP} and PSD_{BULK}.

CONCLUSIONS

The features of the SPP and bulk wave scattering from polycrystalline gold films with different statistical surface characteristics were analyzed. The measurements of the scattering indicatrices showed a significant difference in the relative scattered energy of the surface and volume waves. This difference is due to the local field amplification by almost an order of magnitude upon surface wave excitation and to the differences in the interaction of surface and volume waves with the surface.

A comparison of the relative scattered energy of surface waves with the results of calculation of the multifractal dimension of the gold film surface indicates that the SPP radiative decay intensity depends on both the rms surface roughness and the surface wave propagation length.

The scattering indicatrices demonstrate that an increase in the small-scale roughness leads to an increase in the scattering isotropy and some loss of the structural information about the films. Apparently, this is a consequence of multiple nonradiative SPP scattering, which causes a change in the SPP propagation direction along the surface

It is shown that, in contrast to the bulk wave scattering, the SPP scattering is more sensitive to the film annealing temperature. The comparative analysis of the power spectral density function of surface roughness and the integral and angular dependences of the SPP and bulk wave scattering indicates that surface plasmons undergo a significant multiple nonradiative scattering in gold films.

ACKNOWLEDGMENTS

We are grateful to G.V. Beketov for the program for calculating the optical characteristics of metal films from the angular dependence of the light reflection coefficient under ATIR conditions and to S.A. Zin'o and E.V. Kostyukevich for the help in preparing samples.

REFERENCES

1. J. C. Stover, *Optical Scattering. Measurements and Analysis* (SPIE, Washington, 1995).
2. J. M. Bennett and L. Mattsson, *Introduction to Surface Roughness and Scattering* (OSA, Washington, 1989).
3. V. M. Agranovich and D. L. Mills, *Surface Polaritons. Electromagnetic Waves at Surface and Interfaces* (North-Holland, Amsterdam, 1982).
4. H. Raether, *Surface Plasmons on Smooth and Rough Surfaces and on Gratings* (OSA, Springer-Verlag, 1988).
5. V. Coello, *Elastic Scattering of Surface Plasmon Polaritons* (Aalborg University, Aalborg, 1999).
6. H. Ogura, Z. L. Wang, Y. Sasakura, and V. Freilikher, Opt. Commun. **134**, 1 (1997).
7. S. I. Bozhevolnyi, B. Vohnsen, I. I. Smolyaninov, and A. V. Zayats, Opt. Commun. **117**, 417 (1995).

8. E. Kretschmann, Z. Phys. **241**, 313 (1971).
9. E. Kroger and E. Kretschmann, Z. Phys. **237**, 1 (1970).
10. E. Kretschmann, Opt. Commun. **5**, 221 (1972).
11. S. I. Bozhevolnyi, V. A. Markel, V. Coello, W. Kim, and V. M. Shalaev, Phys. Rev. B **58**, 11 441 (1998).
12. B. A. van Tiggelen, A. Lagendijk, M. P. van Aldaba, and A. Tip, Phys. Rev. B **45**, 12 233 (1992).
13. B. Snopok, P. Strizhak, E. Kostyukevich, V. Serebriy, S. Lysenko, P. Shepeliavii, S. L. Priatkin, S. Kostuykevich, Yu. Shrishov, and E. Venger, Semocond. Phys. Quant. Electron. Optoelectron. **2**, 86 (1999).
14. *NanoScope Command Reference Manual. Digital Instruments* (Veeco Metrology Group, 1999).
15. V. A. Sterligov, P. Cheyssac, S. I. Lysenko, and R. Kofman, Opt. Commun. **177**, 1 (2000).
16. J. M. Elson, J. P. Rahn, and J. M. Bennett, Appl. Opt. **22**, 3207 (1983).
17. V. A. Sterligov and M. Kretschmann, Opt. Express **13**, 4134 (2005).
18. V. A. Sterligov, P. Cheyssac, S. I. Lysenko, and R. Kofman, Opt. Commun. **186**, 27 (2000).
19. P. B. Johnson and R. W. Christy, Phys. Rev. B **6** (12), 4370 (1972).
20. M. Bjuggren, L. Krummenacher, and L. Mattsson, Opt. Eng. **1997**, 874 (1997).
21. Ph. Dumas, B. Bouffakhreddine, C. Amra, P. Vatel, E. Andre, R. Galindo, and F. Salvan, Europhys. Lett. **22**, 717 (1993).
22. J. M. Elson, Phys. Rev. B **30**, 5460 (1984).
23. S. Pichlmaier, K. Hehl, and M. Arnold, Wav. Rand. Med. **6**, 269 (1996).
24. S. I. Bozhevolnyi, Phys. Rev. B **54** (11), 8177 (1996).